

Supporting Information

A Comparative Study of Plasmonic Nanoparticles for Targeted Photothermal Therapy of Melanoma Tumors Using Various Irradiation Modes

Lidia Mikhailova¹, Elizaveta Vysotina¹, Maria Timofeeva¹, Elena Kopoleva¹, Van Gulinyan¹, Olesia Pashina^{1,2}, Konstantin Arabuli¹, Olga Gusliakova^{3,4}, Ekaterina Prikhozhdenko⁴, Xiaoli Qi⁵, Andrey Petrov¹, Eduard Ageev¹, Mihail Petrov¹, Constantino De Angelis², Mikhail Durymanov^{5,6,*}, Gleb Sukhorukov^{3,7}, Mikhail V. Zyuzin^{1,8,*}

¹School of Physics and Engineering, ITMO University, St. Petersburg 191002, Russian Federation

²University of Brescia, Department of Information Engineering, Brescia, Italy

³Vladimir Zelman Centre for Neurobiology and Brain Restoration, Moscow, Russia

⁴Science Medical Center, Saratov State University, Saratov 410012, Russia

⁵Medical Informatics Laboratory, Yaroslav-the-Wise Novgorod State University, Veliky Novgorod, 173003, Russia

⁶Department of Radiochemistry, Faculty of Chemistry, M.V. Lomonosov Moscow State University, Moscow, 119991, Russia

⁷Life Improvement by Future Technologies Center, Moscow, Russia

⁸Qingdao Innovation and Development Center, Harbin Engineering University, Qingdao 266000, Shandong, China

*corresponding authors: mikhail.zyuzin@metalab.ifmo.ru, durymanov.mo@novsu.ru

CONTENT

1. Materials
 - a. For Au NRs synthesis and functionalization
 - b. For cell experiments
 - c. For in vivo experiments
 - d. For histological analysis
2. Numerical simulation of Au NRs optical heating
3. Synthesis of functionalized Au NRs
 - a. Synthesis of Au NRs
 - b. Surface coating of Au NRs with PEG
 - c. Estimation of **Au@PEG** modification extent
 - d. Surface modification Au NRs with peptides
 - e. Estimation of Au NRs coating efficiency with peptides
 - f. Characterization of Au NRs: SEM/TEM/UV-Vis/FTIR
 - g. Optical heating of Au NRs, experimental setup, photothermal conversion efficiency
 - h. Reshaping of Au NRs
 - i. Photoacoustic imaging of phantoms
 - j. Stability in buffers
4. Cell studies
 - a. Hemolysis assay
 - b. Cells
 - c. Melanogenesis assay
 - d. Uptake studies
 - e. Toxicity studies, experimental setup
 - f. Photoacoustic imaging in B16-F10 cells
5. Animal studies
 - a. Animals
 - b. Tumor establishment
 - c. Synchronicity of tumor growth
 - d. Photoacoustic imaging in vivo
 - e. Photothermal therapy, experimental setup
 - f. Histological analysis
6. Clinical studies review
7. References

1. Materials

1 a. For Au NRs synthesis and functionalization

Gold (III) chloride trihydrate ($\text{HAuCl}_4 \cdot 3\text{H}_2\text{O}$, $\geq 99.9\%$, Sigma-Aldrich), ascorbic acid (AA, $\geq 99.0\%$, Sigma-Aldrich), sodium borohydride (NaBH_4 , 98%, Sigma-Aldrich), cetyltrimethylammonium bromide (CTAB, $\geq 99\%$, Sigma-Aldrich), sodium oleate (NaOL, $> 97.0\%$, Sigma-Aldrich), and thiol-PEG-carboxylate (SH-PEG-COOH, M_w 2100, Sigma Aldrich, USA), phosphate-buffered saline (PBS, Biolot, Russia), Ac-SYSMEHRWGKPV-NH₂ ($\text{C}_{68}\text{H}_{100}\text{N}_{20}\text{O}_{18}\text{S}$, M_w 1517.71, PepTech, Russia, **Ac-12**), H-GKRKGS GSSIISHFRWGKPV-NH₂ ($\text{C}_{98}\text{H}_{159}\text{N}_{33}\text{O}_{24}$, M_w 2225.56, PepTech, Russia, **GKR**) were all used without additional purification.

1 b. For cell experiments

Alpha Minimum Essential Medium (Alpha-MEM), trypsinEDTA solution, and phosphate-buffered saline (PBS) were purchased from Biolot (Russia). Antibiotic/Antimycotic Solution (100x) containing penicillin, streptomycin, and amphotericin B was purchased from Capricorn scientific, Germany. Fetal bovine serum (FBS) was obtained from HyClone (USA). Rhodamine B (RhB, $\geq 95\%$) was purchased from Sigma-Aldrich, and Cyanine5 NHS ester (Cy5, $\geq 95\%$) was purchased from Lumiprobe, (GmbH). The AlamarBlue cell viability reagent was purchased from Invitrogen (USA).

1 c. For in vivo experiments

Zoletil (tiletamine hydrochloride 25 mg, zolazepam hydrochloride 25 mg) was purchased from Vibrac animal health, (India). Xyla (xylazine 20 mg) was purchased from Interchemie (The Netherlands). Saline solution (sodium chloride 0.9%) was purchased from Gematek (Russia).

1 d. For histological analysis

Formaldehyde, paraffin, 1% hydrochloric acid solution, methanol, potassium hexacyanoferrate (II) trihydrate, and PBS (phosphate buffered saline) were purchased from Thermo Fisher Scientific (USA). Ehrlich's hematoxylin was purchased from Labiko (Russia). Eosin Y was purchased from Sigma-Aldrich (Germany). The glycergel mounting medium was obtained from Agilent Dako (USA).

2. Numerical simulation of Au NRs optical heating

Simulations were conducted in the COMSOL Multiphysics software package, with the Electromagnetic Waves Frequency Domain module linked to two Partial Differential Equations modules, which modeled the evolution of electron and phonon subsystems.

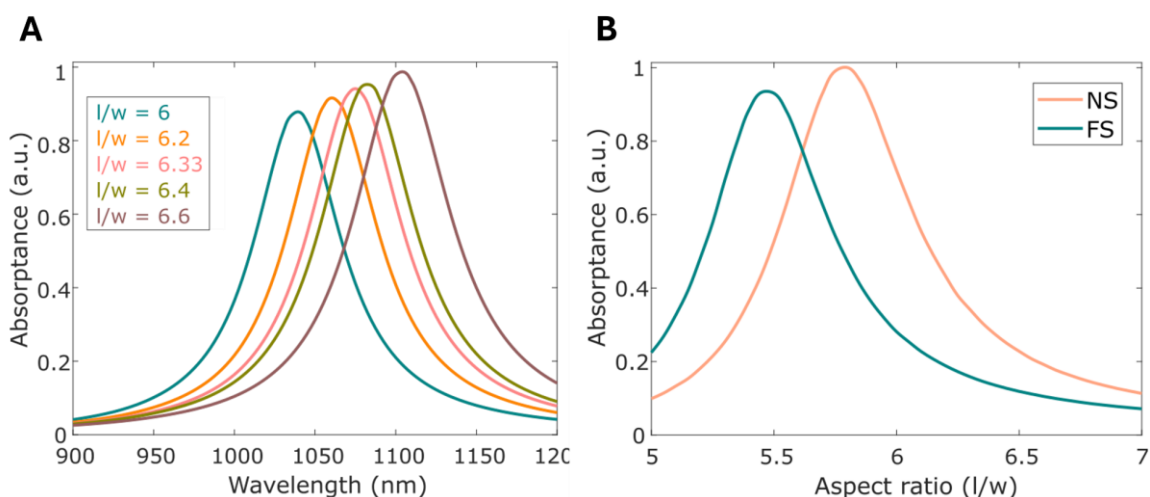


Figure S1. (A) Numerical simulation of absorption spectra for various aspect ratios l/w of a single Au NR suspended in water, with length l and width w . (B) Numerical simulation of absorption vs. the aspect ratio of a single Au NR suspended in water, at fixed wavelengths of FS (1030 nm) and NS (1064 nm) excitation.

3. Synthesis of functionalized Au NRs

3 a. Synthesis of Au NRs

Au NRs were synthesized using the seed-mediated method described previously¹. This process contains two steps. The first step is dedicated to the preparation of the seed solution. For this, 2.5 mL of 0.2 M cetrimonium bromide (CTAB) aqueous solution was added to 2.5 mL of 0.5 mM HAuCl₄ under stirring. Then, an ice-cold freshly prepared solution of 0.01 M NaBH₄ (0.3 mL) was diluted with DW to 0.5 mL for immediate administration to the Au(III) solution under vigorous stirring for 2 min. Note that the color of the resulting mixture immediately changed from strong yellow to brownish. After stirring was stopped, the obtained seed solution was left undisturbed for further use. Important, seed solution should be used between 30 min and 2 h after preparation to avoid aging². Aging is indicated by a change in color from yellowish brown to pink. The second step is the preparation of the growth solution. For this, 0.617 g of sodium oleate NaOL and 4.5 g of CTAB were added to 125 mL of deionized water (DW) in a conical flask and placed in a plate heater (50 °C) under vigorous stirring until dissolved. Thereafter, the obtained solution was cooled to 30 °C, and 18 mL of 4 mM silver nitrate AgNO₃ was added. The resulting solution was cautiously mixed and left without any disturbance for 15 min. Next, 125 mL of 1 mM HAuCl₄ solution was added, and the mixture was finely stirred for 90 min. Then, 1.5 mL of concentrated hydrogen chloride HCl was added to tune the aspect ratio of Au NRs and adjust the power of hydrogen in the solution, which was left for another 15 min stirred. Finally, 0.625 mL of 0.064 M ascorbic acid (AA) was added and quickly stirred for half a minute. Notably, AA as a reducing agent in the presence of CTAB bromide ions changes the color of the growth solution from strong yellow to transparent³. Next, 0.1 mL of the seed solution prepared in the previous step was injected. The

final solution was left for 12 h at 30 °C to form Au NRs. The color of the solution gradually changed from pinkish to violet with ruby opalescence. The next day, the solution of Au NRs was washed by centrifugation (8000 rpm, 30 min) to remove the residue of the chemical reaction and then resuspended in the same volume of DW.

3 b. Surface coating of Au NRs with PEG

Surface modification of Au NRs stabilized with CTAB with SH-PEG-COOH was performed using the ligand exchange method. For this, 30 mL of the previously prepared Au NRs were centrifuged (14000 rpm, 8 min) under heating up to 55 °C to form the CTAB stabilization layer. Then, after the supernatant was removed, 2 mL of 10 mg/mL aqueous SH-PEG-COOH solution was added. Further, Au NRs were ultrasonicated and then centrifuged (14000 rpm, 8 min). After the supernatant was removed, a new volume (2 mL) of SH-PEG-COOH was added. Two milliliters of Au NRs modified with PEG were again ultrasonicated and stored for further use.

3 c. Estimation of Au@PEG modification extent

To verify the presence of PEG on the Au NRs surface, the method described earlier⁴. was used. The supernatant remained after the surface coating procedure was collected. Then, barium chloride solution (5% (w/v) solution was prepared by dissolving the salt in 1 M hydrochloric acid. The iodine solution was prepared by dissolving 0.635 g of iodine in 50 mL of 2% (w/v) potassium iodide. Afterwards, 200 µL of barium chloride solution and 100 µL of iodine solution were added to 800 µL of the supernatant solution. The solution was resuspended and left undisturbed for 15 min until coloration occurred. Finally, the absorbance of the solution was measured at 535 nm using a Shimadzu UV-3600 spectrophotometer. A similar procedure was performed using a range of PEG solutions with known concentrations to obtain a calibration curve. The amount of PEG on the surface of the Au NRs was calculated as the difference between the amount of PEG added to the Au NRs and the amount of PEG remaining in the supernatant:

$$M = \frac{(m_{PEG} - (m_1 + m_2)) \times 100\%}{m_{PEG}}$$

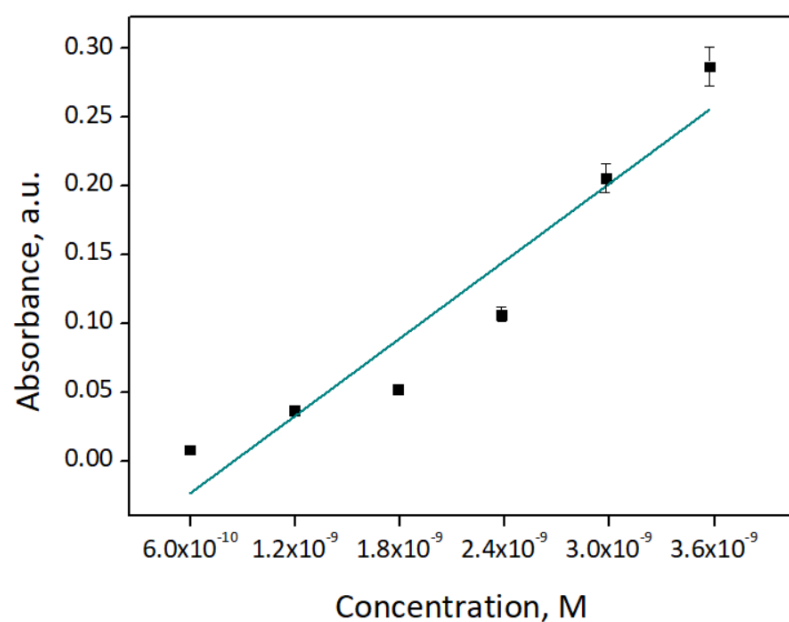


Figure S2. Absorbance of SH-PEG-COOH at 535 nm at different concentrations.

Table S1. Estimation of the surface modification extent of Au NRs with SH-PEG-COOH.

| | Amount of SH-PEG-COOH added (mg) | Amount of SH-PEG-COOH in the supernatant (mg) | Amount of SH-PEG-COOH in the supernatant (%) |
|----------------------------------|----------------------------------|---|--|
| Washing step 1 | 10 | 5.18×10^{-2} | 0.518% |
| Washing step 2 | | 4.15×10^{-3} | 0.0415% |
| Total modification extent | | | 99.4% |

3 d. Surface modification Au NRs with peptides

The modification of **Au@PEG** was performed using two α MSH-like peptides including Ac-12 (Ac-Ser-Tyr-Ser-Met-Glu-His-Arg-Trp-Gly-Lys-Pro-Val-CONH₂) with two primary amines (M_w 1517.71 g/mol, extinction coefficient $6970 \text{ M}^{-1} \text{ cm}^{-1}$), and GKR (Ac-Gly-Lys-Arg-Lys-Gly-Ser-Gly-Ser-Ser-Ile-Ile-Ser-His-Phe-Arg-Trp-Gly-Lys-Pro-Val-CONH₂) with four primary amines (M_w 2225.56 g/mol, extinction coefficient $5690 \text{ M}^{-1} \text{ cm}^{-1}$).

For modification of **Au@PEG** with Ac-12 and GKR peptides, surface activation has been first performed⁵. For this aim, previously synthesized **Au@PEG** were resuspended by sonication and then centrifuged to remove excess unreacted PEG in the store solution. The sediment was

dispersed in 2 mL of a 5 mM PBS buffer (pH 7.4) and sonicated for several minutes at room temperature. The final concentration of **Au@PEG** was estimated spectrometrically as 150 µg/mL. Then, to catalyze the formation of amide bonds between carboxyl and amine groups and stabilize the formation of functional groups, N-(3-dimethylaminopropyl)-N'-ethyl carbodiimide hydrochloride (EDC) (Sigma-Aldrich, St. Louis, MO) (20 mM) and N-hydroxysulfosuccinimide sodium salt (Sulfo-NHS) (Sigma-Aldrich, St. Louis, MO) (40 mM) were added to 2 mL of PEGylated Au NRs suspension and stirred for 30 min. After centrifugation and removal of excess EDC/NHS, the precipitates were finally resuspended in the same volume of PBS, and the total volume was divided equally into two 2-mL tubes. Then, 3.57 mg of Ac-12 and 5 mg of GKR were added to the particle suspension followed by 2 h stirring at room temperature. After peptide modification, the particles were collected by centrifugation at 12,000 rpm for 10 min and washed with PBS. The supernatant with unreacted peptides after the reaction was used for further detection of unreacted peptides.

3 e. Estimation of Au NRs coating efficiency with peptides

The modification ratio of peptide (% w/w) was determined by the detection of unreacted primary amino groups⁶ in peptides after the addition of fluorescamine (Sigma-Aldrich, St. Louis, MO). Briefly, after Au NR functionalization with peptides, the particles have been centrifuged to remove the unreacted peptide. Then, 100 µL of supernatant after nanoparticle sedimentation was mixed with 30 µL of solution of fluorescamine in DMSO (3 mg mL⁻¹). Non-fluorescent fluorescamine instantly reacts with primary amino groups at room temperature in aqueous medium, resulting in a highly fluorescent product. Fluorescence intensity was measured using a CLARIOstar PLUS plate reader (BMG Labtech, Offenburg, Germany) at $\lambda_{ex} = 395$ nm and $\lambda_{em} = 495$ nm. To obtain a calibration curve, standard solutions of the peptide with known concentrations were prepared in PBS. The concentration of peptide in all supernatant samples was determined by comparison with the calibration plot for free peptide (**Fig. S3**). The labeling ratio of peptides (% w/w) was calculated as follows:

$$P = \frac{W_{attached\ peptide}}{W_{Au@PEG} + W_{attached\ peptide}} \times 100,$$

where $W_{attached\ peptide} = W_{before\ reaction} - W_{supernatant}$

$W_{before\ reaction}$ is the weight of peptide at the beginning of reaction, and $W_{supernatant}$ is the weight of unreacted peptide.

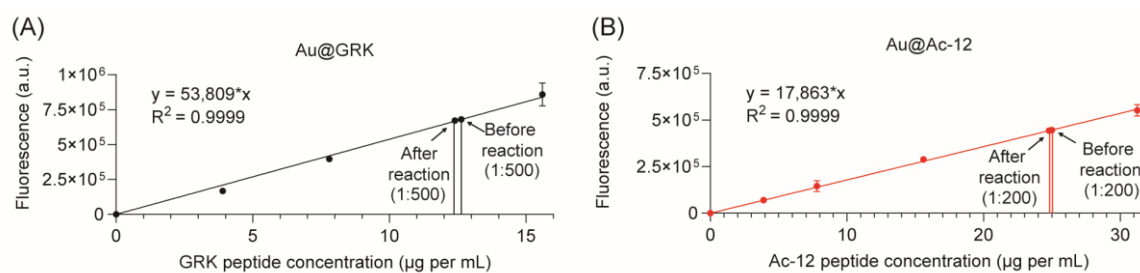


Figure S3. Calibration plots for free (A) GRK and (B) Ac-12 peptides upon fluorescamine reaction with plotted values, obtained for the supernatants before and after the reaction of peptide conjugation with Au NRs.

3 f. Characterization of Au NRs

Scanning electron microscopy (SEM)

Geometry of Au NRs were analyzed using a LIBRA 200 FE HR, Carl Zeiss (accelerating voltage in the range between 80 kV and 200 kV). For sample preparation, an aqueous solution of Au NRs in the volume of 3 µL was placed on a silicon plate and left to dry overnight. The next day the dry sample was used for visualization.

Transmission electron microscopy (TEM)

The parameters of the crystal lattice of the obtained Au NRs were revealed using the STEM regime of a LIBRA 200 FE HR, Carl Zeiss. Aqueous solution of Au NRs (3 µL) placed on a copper grid were used to obtain a convergent beam electron diffraction pattern, which proves the Au(100) crystalline structure of the nanorods. Based on TEM analysis, Au NRs size distribution statistics was revealed. For this, totally 110 Au NRs were analyzed.

Energy-dispersive X-ray spectroscopy (EDX)

EDX spectra of the obtained Au NRs were measured to verify their elemental composition. For this, dried samples were analyzed using a LIBRA 200 FE HR, Carl Zeiss and a JEOL Centurio energy-dispersive 1sr X-ray spectrometer (EDXS). Signal accumulation lasted for 5 min. The obtained EDX spectrum shows characteristic peaks for Au and Cu, where the last compound is the copper grid material.

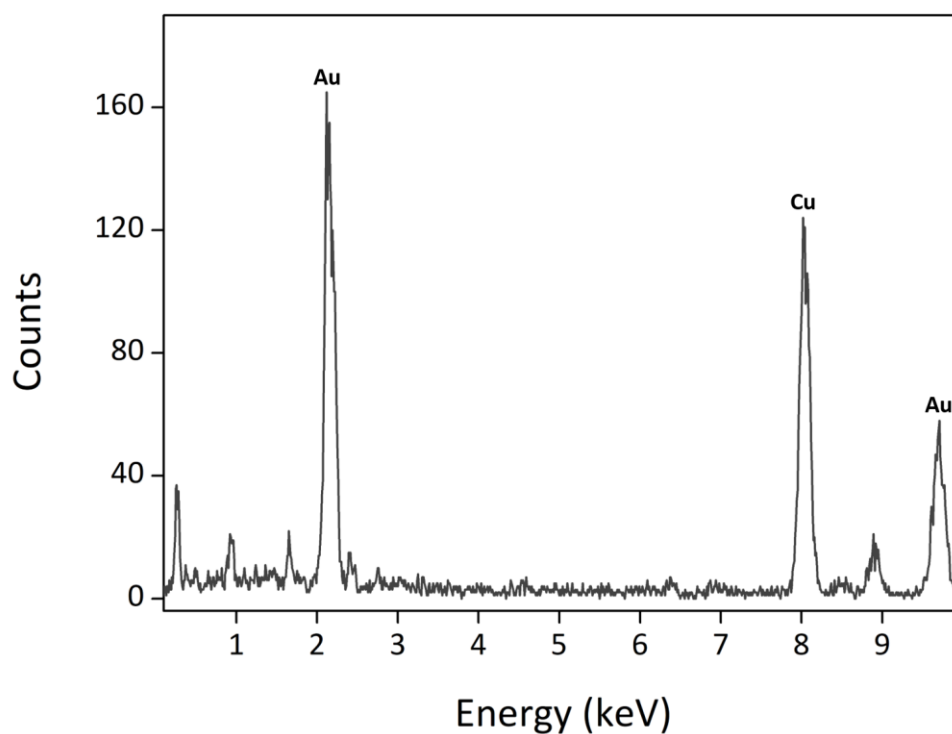


Figure S4. EDX spectrum of Au NRs.

UV-Vis spectroscopy of Au NRs

The absorption spectrum of the aqueous solution of Au NRs was obtained using a Shimadzu UV-3600 spectrophotometer. The range of wavelengths was 400–1300 nm. The solution (3 mL) was poured into a 10-mm path quartz cuvette.

To estimate the concentration of Au NRs in the solution, Bouguer-Lambert-Beer law was used. The extinction coefficient for Au NRs was adopted from a previously published study⁷: $\varepsilon \approx 10^9 \text{ M}^{-1} \text{ cm}^{-1}$. The value of absorption was taken from the obtained absorption spectrum.

The concentration was calculated as follows:

$$C = \frac{A}{\varepsilon \cdot l} = \frac{0.772}{10^9 \text{ M}^{-1} \text{ cm}^{-1} \cdot 1 \text{ cm}} = 0.761 \cdot 10^{-9} \text{ M}$$

Fourier transform infrared spectroscopy (FTIR)

Fourier transform infrared spectra were collected on a TENSOR II FTIR Spectrometer (Bruker Optics, Germany) by scans in the range from 400 to 4000 cm^{-1} with a resolution of 1 cm^{-1} . Dried **Au@PEG**, **Au@Ac-12**, **Au@GKR** samples (0.5-1 mg) were placed into a sample holder and analyzed.

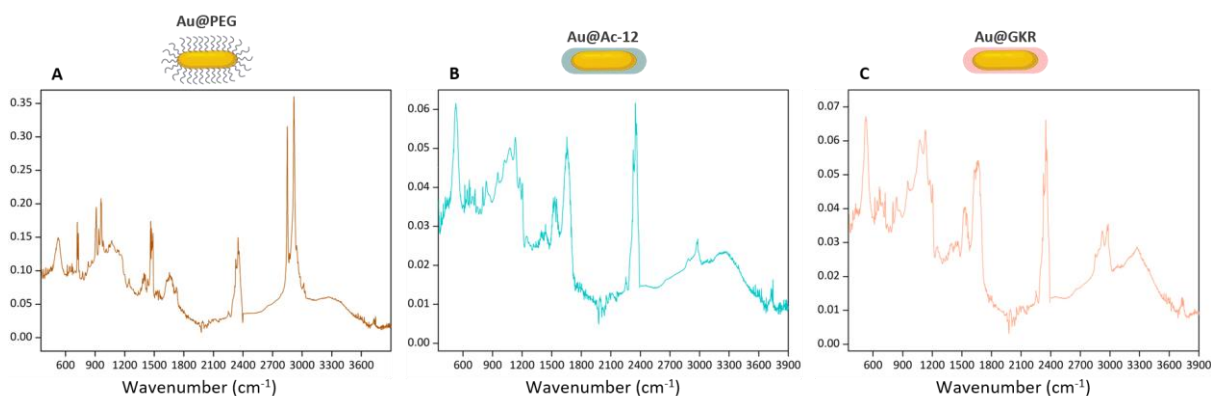


Figure S5. Fourier transform infrared spectrums of (A) **Au@PEG**, (B) **Au@Ac-12**, (C) **Au@GKR**.

3 g. Optical heating of Au NRs, experimental setup, photothermal conversion efficiency

To assess the photothermal conversion efficiency of the Au NRs, a procedure was conducted as described previously⁸. First, 2 mL of **Au@PEG** at a concentration of 150 µg/mL was introduced into a quartz cuvette with an optical path length of 10 mm. Subsequently, the cuvette was exposed to irradiation using an ytterbium fiber laser IRE-POLUS ILMI-1-50 (1064 nm, 100 kHz, <140 ns) and an ytterbium fiber laser Antaus Avesta (1030 nm, 200 kHz, <250 fs). Following a 20-min irradiation, the laser was deactivated, allowing the cuvette to naturally cool to ambient temperature over an additional 20 min. Throughout the experiment, the temperature of the cuvette was continuously monitored using an FLIR Titanium 520 M infrared thermal imaging camera (**Figure S6A**).

The laser irradiation power was determined using an advanced laser power meter (StarBright). The power density was then calculated as follows: $P_d = P/S$, where P is the measured power and S is the area of the laser spot.

To investigate the temperature increase for different concentrations of **Au@PEG**, the same setup was used. First, 1 mL of **Au@PEG** with a range of concentrations (75-300 µg/mL) was placed into a quartz cuvette with an optical path length of 10 mm. The cuvette was irradiated by both types of lasers with a range of power densities (0–8200 mW/cm²). The irradiation lasted for 180 s, and the heating process was observed using an infrared thermal imaging camera.

To calculate conversion efficiency the following equations was used:

$$\eta = \frac{hS(T_{max} - T_{min}) - Q_{dis}}{I(1 - 10^{-A_{1030/1064}})}$$

where h is the heat transfer coefficient, S is the surface area of the cuvette, and T_{max} and T_{min} are the highest (45.7 and 37.4 °C) and lowest (23 °C) ambient temperatures reached during the

experiments with laser power I equal to 1 W. To describe the heat dissipation due to light absorption by an aqueous solution, a parameter Q_{dis} was introduced. The measured adsorption for **Au@PEG** at 1030 nm was equal to 3.50, and at 1064 nm, to 4.92. The term hS can be defined as:

$$hS = \frac{m \cdot C}{\tau_s}$$

where m is the mass of the sample, equal to 1g, C is the heat capacity, equal to 4.2 J/g · °C, τ_s is the relaxation time of the system, which starts with the process of cooling, which can be found as:

$$\tau_s = - \frac{t}{\ln \left(\frac{T_{current} - T_{min}}{T_{max} - T_{min}} \right)}$$

where θ is equal to:

$$\theta = \frac{T_{current} - T_{min}}{T_{max} - T_{min}}$$

Therefore, the relaxation times of the system for both lasers were found by linearly fitting the data (**Figure S6B**), and they were equal to 422.07 for the ytterbium fiber laser IRE-POLUS ILMI-1-50 (1064 nm, 100 kHz, <140 ns) and 228.14 for the ytterbium fiber laser Antaus Avesta (1030 nm, 200 kHz, <250 fs). Thus, the term hS can be found by substituting the relaxation time to the equation defining the hS summand, and it is equal to 10.05 mW for FS laser and 18.04 mW for NS laser. Q_{dis} is equal to 404 mW, and it was measured independently for a quartz cuvette that contained distilled water. After calculating all the summands, the photothermal conversion efficiency was equal to 22.7% and 26.4%.

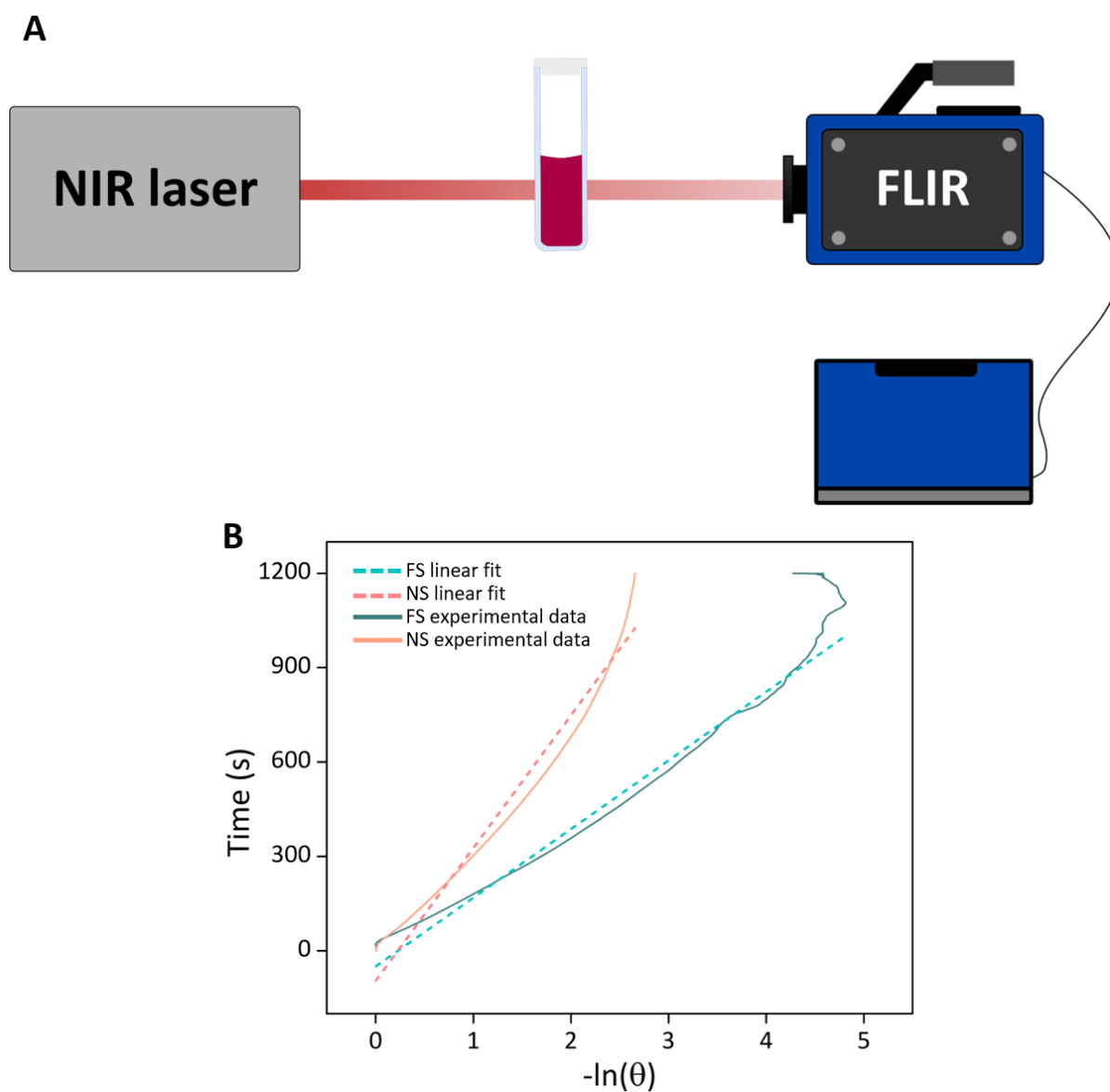


Figure S6. (A) Schematic illustration of the experimental setup for the estimation of **Au@PEG** photothermal conversion efficiency. (B) Time data of $-\ln(\theta)$ calculated for the period of cooling.

3 h. Reshaping of Au NRs

To study the reshaping of **Au@PEG** after irradiation with FS and NS (up to 8800 mW/cm^2) 9 samples were examined: one for control without irradiation, 4 for power range of FS pulses and 4 for power range of NS pulses. Each sample contained 1 mL of **Au@PEG** with known $150 \text{ }\mu\text{g/mL}$ concentration.

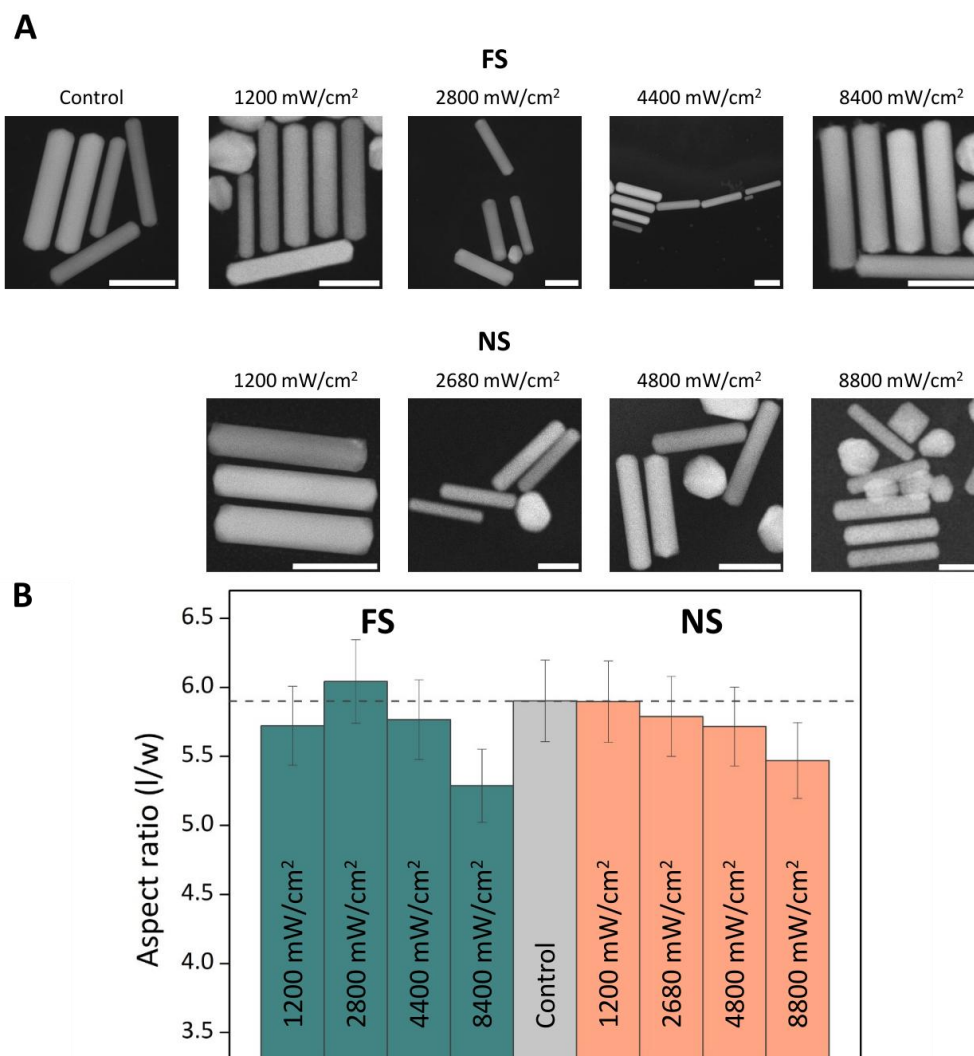


Figure S7. Effect of femtosecond and nanosecond laser irradiation on the structure of Au NRs. A. Representative TEM images of **Au@PEG**, scale bar corresponds to 50 nm. B. Change of aspect ratio of **Au@PEG** after laser irradiation with FS and NS.

3 i. Photoacoustic imaging

To study the dependence of the photoacoustic signal intensity on the concentration of Au NRs, agarose phantoms simulating aqueous medium were made. For this purpose, low melting point agarose powder (0.1 g) (TopVision, Thermo Scientific, USA) was added to 10 mL of deionized water. The solution was then heated to 70 °C for half an hour to dissolve the powder completely and uniformly. Next, the agarose gel and Au NRs solution were combined and vigorously mixed under sonication to obtain the final nanoparticle concentrations: 0 (empty tube), 500, 1000, 2000, 4000, and 6000 µg/mL.

The photoacoustic signal was captured using the TriTom (Photosound, USA) imaging platform. An excitation wavelength of 1064 nm (pulse energy 80 mJ, laser power density 140 mW/cm²) was used to excite the Au NR signal (**Figure S8**). Eppendorf tubes containing agarose phantoms were placed in an imaging chamber filled with deionized degassed water at 23°C for all measurements.

During the experiment, the samples were rotated at a rate of 10 degrees per second until a complete rotation. After the measurement, 3D reconstruction of samples was performed with TriTom Imaging GUI v.1.1.12 (PhotoSound Technologies, Inc., USA). Signal inhomogeneities in the samples are due to the inhomogeneity of gel solidification in the presence of air cavities.

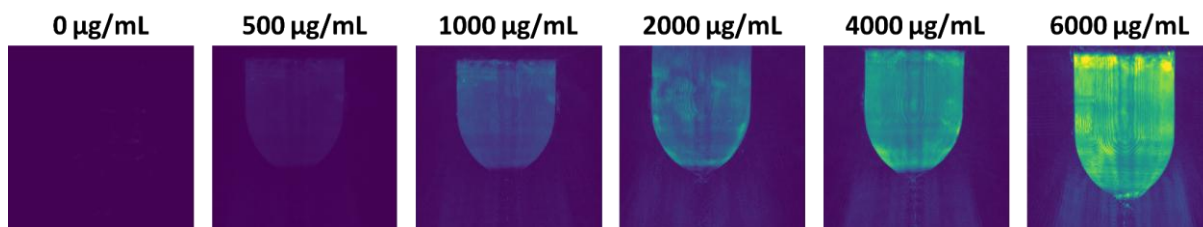


Figure S8. Photoacoustic images of **Au@PEG** phantoms prepared in agarose gel at different concentrations.

After image acquisition, post-processing was performed using ImageJ software. For each sample, an area of 100x100 pixels was selected, for which a histogram of weighted pixel intensities was constructed. The calibration curve of the photoacoustic signal dependence on the Au NRs concentration (**Figure 6B**) was plotted using the obtained data.

3 j. Stability in buffers

To investigate the stability of **Au@Ac-12** and **Au@GKR** at different pH levels (5, 7.2, 9), a Photocor Complex (Photocor, Russia) (4.0 mW HeNe laser, 633 nm) was used. The change in the hydrodynamic diameter was analyzed for several time points (0, 4, 8, 16, and 24 hours). To prepare samples, 100 µL of the synthesized NRs was diluted in 1 mL of the used medium.

The zeta potential values of **Au@PEG**, **Au@Ac-12**, and **Au@GKR** were also measured. The samples (200 µg/mL) were diluted 100-fold in MilliQ water and then measured using a Zetasizer Nano ZS90 (Malvern, UK) equipped with a 4.0 mW HeNe laser operating at a wavelength of 633 nm. The values of zeta potentials are presented in Table **S2**.

Table S2. Zeta potentials of **Au@PEG**, **Au@Ac-12**, **Au@GKR** dispersed in water.

| Sample | ζ potential (mV) |
|----------|------------------------|
| Au@PEG | -14.07 |
| Au@Ac-12 | -0.69 |
| Au@GKR | -1.37 |

4. Cell studies

4 a. Hemolysis assay

A hemolysis assay (**Figure S9**) was conducted to evaluate the biocompatibility of the Au NRs. Human erythrocytes (RBC) were isolated from whole blood (4 mL) using Ficoll solution (4 mL). Subsequently, the mixture of blood and Ficoll was centrifuged for 20 min at 300 g. After centrifugation, sedimented erythrocytes (2 mL) were collected from the bottom of the tube and poured with 3 mL of PBS to wash them (5 min, 300 g). After erythrocytes were resuspended in PBS, **Au@Ac-12** and **Au@GKR** were added to the erythrocytes. The final concentrations of **Au@Ac-12** and **Au@GKR** were 50, 100, 200, and 300 $\mu\text{g}/\text{mL}$. RBCs were incubated with modified Au NR for 2 h and then centrifuged (5 min, 300xg). As a positive control, RBC lysis buffer was used, and as a negative control, PBS buffer was used. The extracted hemoglobin concentration in the supernatant was measured using a Shimadzu UV-3600 spectrophotometer at 540 nm.

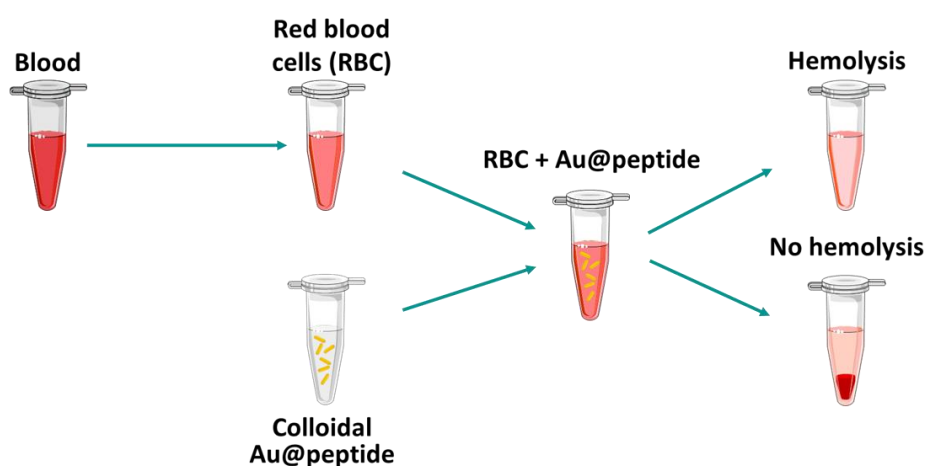


Figure S9. Scheme of the hemolysis procedure.

4 b. Cells

A murine melanoma cell line (B16-F10) was obtained from the American Type Culture Collection (ATCC). Cells were cultured in AlphaMEM with 10% of vol. FBS supplement and 1% of vol. antibiotic/antimycotic solution. The cells were maintained in a sterile humidified atmosphere (5% CO_2) at 37°C.

4 c. Melanogenesis assay

To estimate the efficiency of melanin production, a melanogenesis assay was performed. First, murine melanoma B16-F10 cells were seeded in a 96-well plate at a density of 2×10^3 cells per well. This initial seeding density is optimal for subsequent treatment and measurement of melanin production. The following day, different test compounds — Ac-12, GKR, **Au@PEG**, **Au@Ac-12**, and **Au@GKR** — were added to the cells. These compounds were introduced in a range of peptide-based concentrations from 10^{-3} to 1 $\mu\text{g}/\text{mL}$. This concentration gradient allows the assessment of dose-dependent effects on melanin production. After adding the test compounds, the

cells were incubated for 48 h. This incubation period is sufficient for the compounds to exert their effects on melanogenesis, allowing for the evaluation of melanin synthesis.

After incubation, the medium containing the expressed melanin was carefully transferred to another plate. This step is critical because it separates the melanin produced by cells from the cellular debris, ensuring that subsequent measurements only reflect the melanin content. The melanin signal in each well was detected spectrometrically at an absorbance wavelength of $\lambda_{\text{abs}} = 405$ nm using a plate reader. This wavelength was chosen because melanin effectively absorbs light in this wavelength range, allowing for accurate quantification of melanin levels. Finally, the level of light absorption was plotted against the concentration of added compounds.

The table with the obtained EC50 values is presented below (**Table S3**).

Table S3. EC50 values for original peptides and modified Au NRs.

| Ac-12 | GKR | Au@Ac-12 | Au@GKR |
|---------------------------|---------------------------|---------------------------|---------------------------|
| 0.281 $\mu\text{g/mL}$ | 0.304 $\mu\text{g/mL}$ | 0.046 $\mu\text{g/mL}$ | 0.058 $\mu\text{g/mL}$ |

4 d. Uptake studies

To visualize the association of Au NRs with B16-F10 cells, cells were seeded in confocal cell imaging dishes ($d = 35$ mm, BIOFIL, China) at a density of 1.0×10^5 cells per dish. Seeded cells were left at 37°C and 5% CO_2 for 24 h. The next day, **Au@PEG**, **Au@Ac-12**, and **Au@GKR** were added to the cells at a concentration of $150 \mu\text{g/mL}$ in 2 mL of cell medium and left overnight. The following day, the cells were washed with PBS to remove the old cell medium and non-associated particles. Then, PBS was removed and replaced with 1 mL of 10% formalin solution. The cells were left for 40 min at room temperature for their fixation. Immediately after that, formalin was removed and replaced with 1 mL of PBS buffer. Thereafter, $50 \mu\text{L}$ of rhodamine B (RhB) solution was added to stain the cells. After 10 min, stained cells were washed with PBS and visualized using a confocal laser scanning microscope Zeiss LSM 710 CLSM (Germany). The confocal aperture was set to 1 Airy unit, and the images were acquired with a 10x objective.

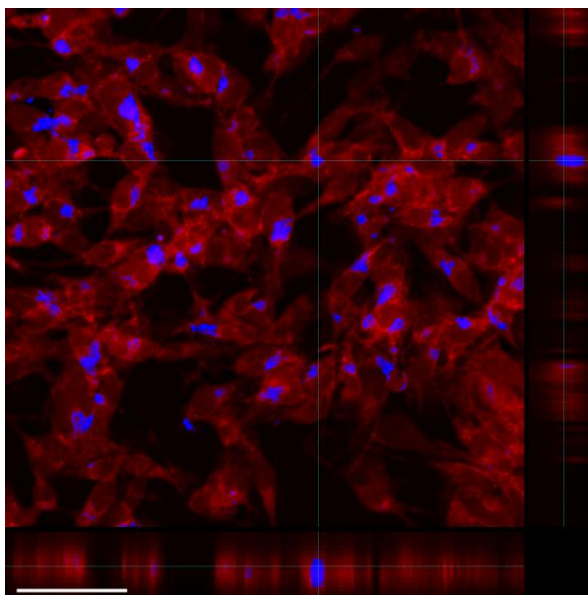


Figure S10. Orthogonal view from X-Y, Y-Z, and X-Z planes of the CLSM image demonstrating uptake of **Au@Ac-12** by B16-F10 cells. Scale bar corresponds to 30 μm .

4 e. Toxicity studies in vitro, experimental setup

B16-F10 cells were seeded in a 6-well plate (1.0×10^6 cells per well). The following day, either **Au@Ac-12** or **Au@GKR** was added to each well at different concentrations (from 75 $\mu\text{g}/\text{mL}$ to 300 $\mu\text{g}/\text{mL}$). The final volume of cell medium in each well was 1.5 mL. After 24 h, cells were washed twice with PBS to remove non-internalized Au NRs. The cells were detached, centrifuged, and resuspended in 100 μL of cell medium to imitate the tumor. The cells were transferred into 600 μL microtubes and positioned in the optical setup.

The cytotoxicity of Au NRs at varying concentrations, laser pulse durations, and power densities was assessed using the experimental setup shown in (**Figure S11**). Laser-induced hyperthermia was generated using a pulsed near-infrared 1030 nm femtosecond Yb:YAG laser Antaus Avesta (200 kHz, <270 fs) and a pulsed near-infrared 1064 nm nanosecond Yb:YAG laser IRE-POLUS ILMI-1-50 (100 kHz, <140 ns) at different power densities ($725 \pm 20 - 5200 \pm 50 \text{ mW}/\text{cm}^2$ for FS; $650 \pm 15 - 6000 \pm 20 \text{ mW}/\text{cm}^2$ for NS). The laser spot area was 0.7 cm^2 . The cells were irradiated for 3 minutes. Temperature changes were captured by an infrared thermal imaging camera FLIR Titanium 520 M operating at a 2 Hz frame rate within a temperature range of 20°C to 57°C.

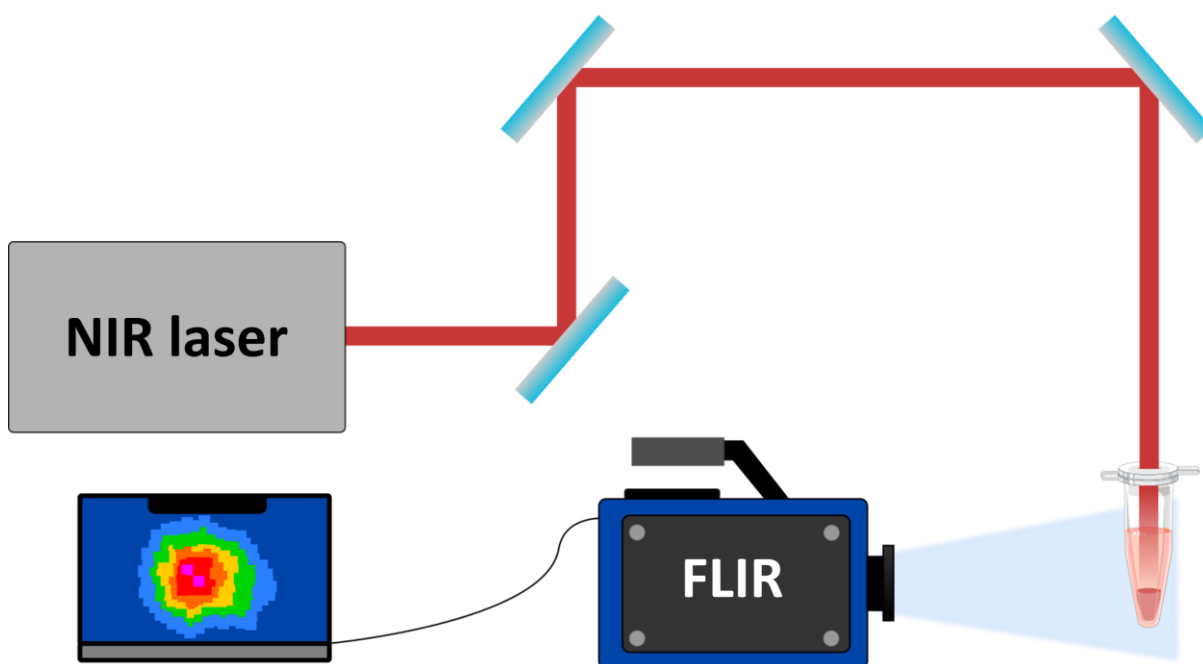


Figure S11. Schematic illustration of the experimental setup for the laser-induced heating of **Au@Ac-12** and **Au@GKR** associated with B16-F10 tumor cells.

4 f. Photoacoustic imaging in B16-F10 cells

B16-F10 cells were seeded on Petri dishes (35 mm) at a density of 1×10^6 cells per dish and left at 37° C in a humidified atmosphere containing 5% CO₂ for 8 h. After the indicated time, the culture medium was aspirated. Then, **Au@PEG** was added to the Petri dishes together with a complete culture medium (the total volume added to the Petri dish was 2 mL, of which 1980 μL of medium and 20 μL of **Au@PEG**, 150 μg/mL concentration). Cells and Au NRs were co-incubated overnight (12 h), followed by washing and replacement of the medium with fresh medium that did not contain AuNRs. As a control, cells were maintained without addition of Au NPs. Photoacoustic imaging in cells was performed immediately after incubation with Au NPs for 12 and 24 h. For measurements, cells were detached using Trypsin-EDTA (0.25%) and washed once with DPBS (Ca-, Mg-free). Centrifugation was performed for 5 min at 800 g. After washing, the cells were pelleted by centrifugation, and DPBS was aspirated. For each time point, 4 experimental cell pellets (after co-incubation with Au NP) and 2 control cell pellets (incubation in AuNP-free culture medium) were prepared.

The photoacoustic images of cells treated with **Au@PEG** were obtained using a TriTom tomograph (PhotoSound Technologies, Inc., Houston, TX, USA) equipped with a PhotoSonus pulsed laser (Ekspla, Vilnius, Lithuania). All measurements were conducted using distilled water (36 °C) as the acoustic coupling medium. Cells in 1.5 mL Eppendorf tubes were placed into the holder and submerged in a distilled water-filled tank alongside an ultrasonic transducer array. The 1064-nm high-energy mode of the PhotoSonus laser was used for photoacoustic excitation. The

ADC gain was set to 25 dB. The 3D photoacoustic images were reconstructed with $0.1 \times 0.1 \times 0.1$ mm voxel size using TriTom software (PhotoSound Technologies, Inc., Houston, TX, USA).

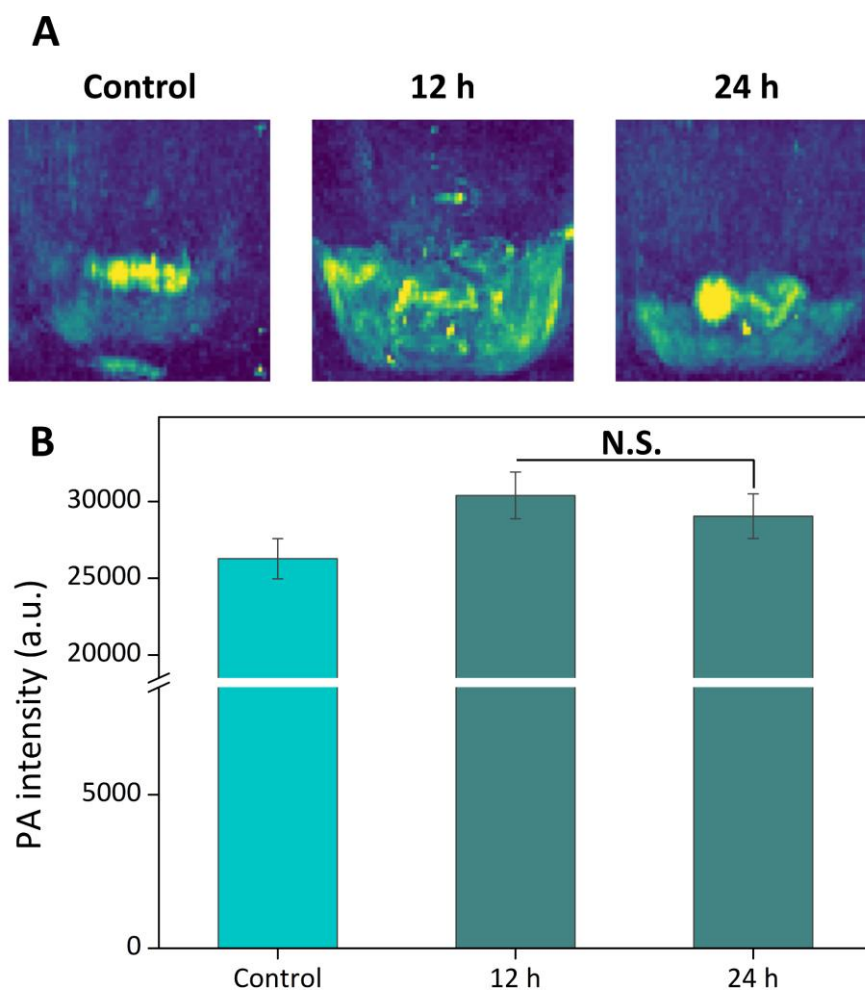


Figure S12. Photoacoustic images of B16-F10 cells incubated with **Au@PEG** for 12 or 24 h. Cells without incubation with **Au@PEG** were used as control. B. PA intensity derived from PA images for all samples (the symbol N.S. indicates no significant differences between signals).

5. Animal studies

5 a. Animals

For *in vivo* studies, healthy C57BL/6 mice (males, 8-week-old, 18-22 g) were purchased from St. Petersburg center of laboratory animals "Rappolovo" of the national research center "Kurchatov Institute". The mice were used for two types of experiments: photoacoustic investigation of bio-distribution and photothermal therapy. The laboratory animals were treated according to the rules of Saratov State Medical University (Ethics Committee Protocol No. 8, dated 7th of March 2023) and the Geneva Convention of 1985 (International Guiding Principles for Biomedical Research Involving Animals). The mice were housed in plastic cages at 22-24 °C and humidity of 40-60% under light/dark conditions for at least 14 days of quarantine, with free access to pellet food and water ad libitum. Quarantined in a specific pathogen-free environment.

5 b. Tumor establishment

To induce melanoma, B16-F10 mouse melanoma cells (CRL-6475 line) were used in C57BL/6 mice (males, 8-week-old, 18-22 g). Briefly, cells were harvested by trypsinization during the exponential growth phase. Cells were then washed twice with ice-cold PBS and resuspended in PBS at a concentration of 1×10^6 cells/mL for 24 h. Subsequently, cells (50 μ L at a concentration of 1×10^6 cells/mL) were promptly subcutaneously injected into the legs of C57BL/6 mice (1 day). Seven days after tumor establishment (7 d) mice were inspected and animals with a sufficient size of the tumor (approximately 2.5 ± 0.3 cm³) were used for further experiments.

5 c. Synchronicity of tumor growth

After injecting 2.5×10^5 cells into the thighs of 5 mice, the external visible dimensions of the tumor were measured in the mice on day 7. For each tumor, 2 diameters were measured, and the tumor area was calculated using the following area formula for an ellipse: $S = \pi \cdot (d_1/2) \cdot (d_2/2)$. The mean tumor area was 4.36 ± 0.63 mm² (**Figure S13**). The calculated coefficient of variation was 14.51%, from which we can conclude that by day 7 before Au NRs injection, the mice had tumors fairly close in size.

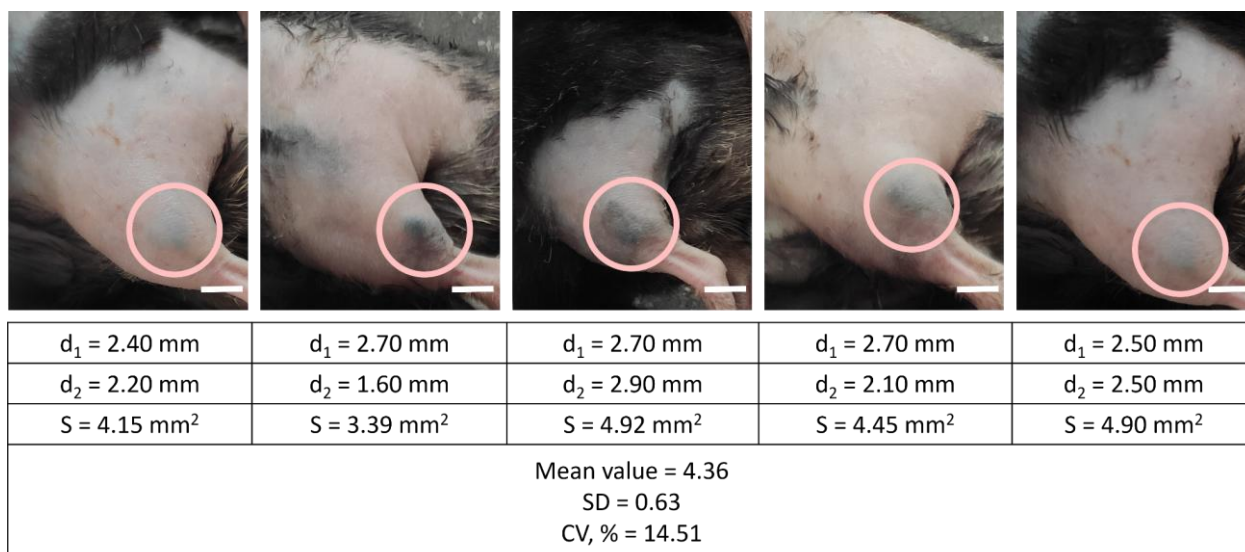


Figure S13. Digital images of mice with injected B16-F10 cells (7 days post injection) illustrating synchronicity of tumor growth.

5 d. Photoacoustic imaging in vivo

The animals imaged on the TriTom imaging platform were injected with a 100 μ L dose of 100 μ g/ μ L **Au@Ac-12** or **Au@GKR**. Prior imaging, the animals were anesthetized with a mixture of zoletil and xyla in 0.9% NaCl, shaved with a trimmer and depilatory cream. Then, the mouse is placed in the frame holder, and the paws are held with soft fasteners. The mouse's head is secured with its front teeth on a horizontal holder, and air is delivered directly through a tube. Mice were placed in a tank filled with deionized water, alongside an ultrasonic transducer array. A pulsed OPO laser (PhotoSonus, Ekspla, Lithuania), tuned to a wavelength of 1064 nm (pulse

energy 80 mJ), was used for photoacoustic excitation. The sample was rotated at a velocity of 10 degrees per second during the measurement. 3D photoacoustic images were then reconstructed using TriTom software (PhotoSound Technologies, Inc., Houston, TX, USA), with a voxel size of 0.1 x 0.1 x 0.1 millimeters.

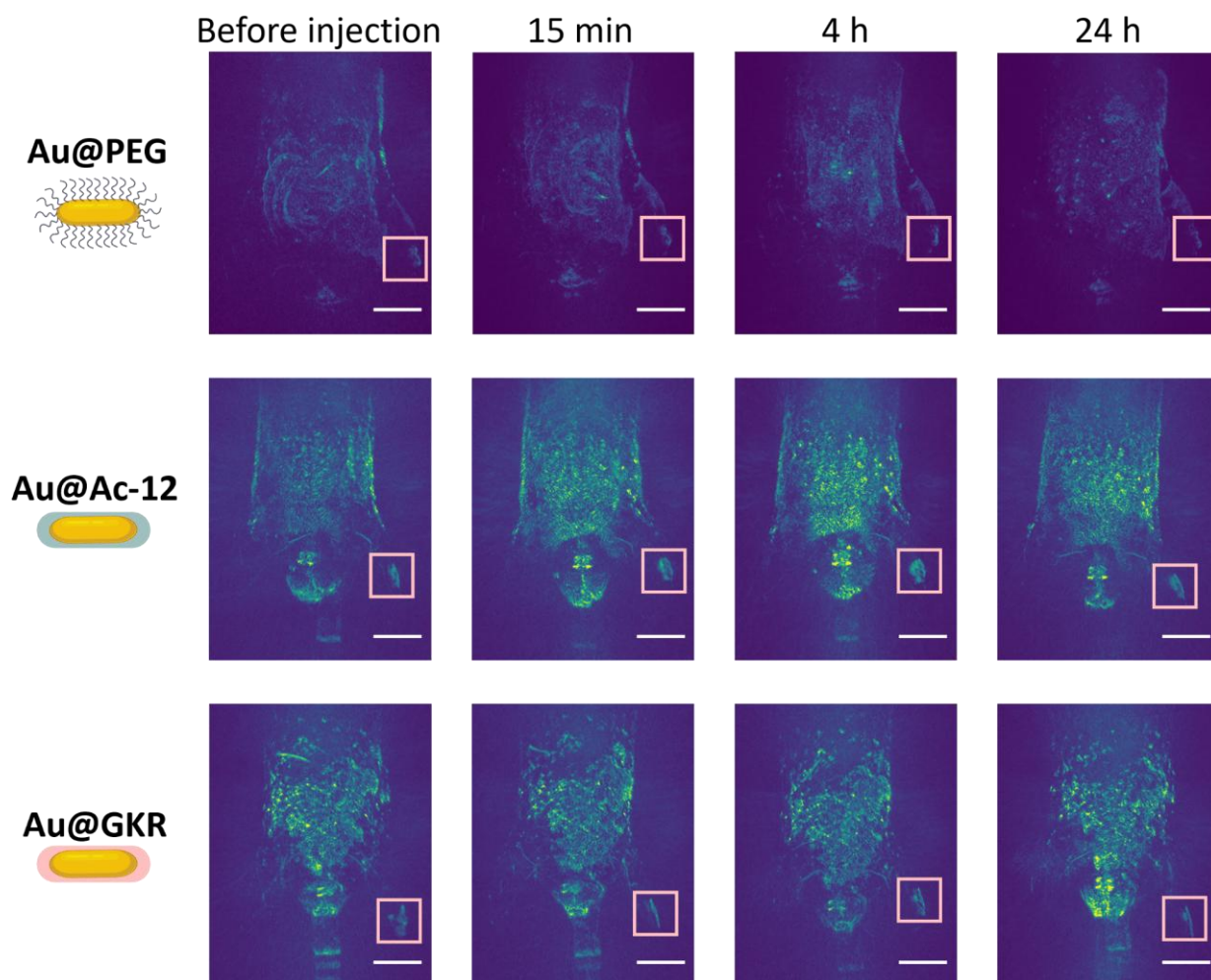


Figure S14. Photoacoustic scans of mice before and after the injection (15 min, 4 h, and 24 h) of 100 μL , 1000 $\mu\text{g}/\text{mL}$ of (from top to bottom) **Au@PEG**, **Au@Ac-12**, **Au@GKR**. Scale bar corresponds to 1 cm.

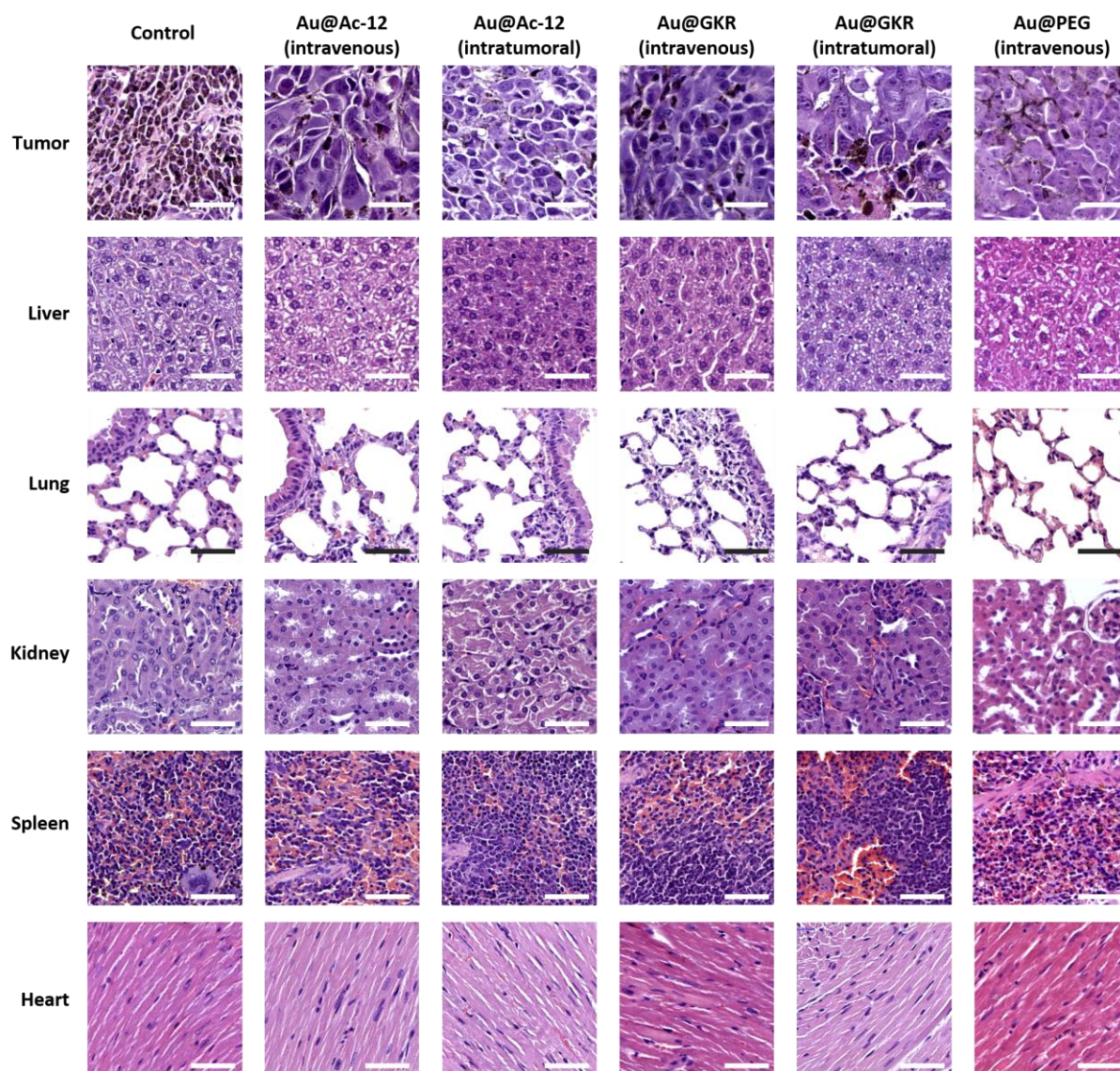


Figure S15. Histological analysis of main organs and tumors 24 h after either intratumoral or intravenous injection of **Au@PEG**, **Au@Ac-12**, **Au@GKR** without laser irradiation. Scale bar corresponds to 50 μm .

5 e. Photothermal therapy, experimental setup

B16-F10 tumor-bearing C57BL/6 mice were divided into four groups for each type of impact for photothermal therapy experiments. The groups were the same for each type of laser irradiation (either FS or NS): (i) control with 0.9% NaCl, (ii) control with NaCl with laser irradiation, (iii) intravenously injected (in the tail vein) **Au@Ac-12** (100 μg NRs in 100 μL), and (iv) intravenously injected (in the tail vein) **Au@GKR** (100 μg NRs in 100 μL). The mice were then irradiated 15 min, 4 h, and 20 h after the injection either with an FS laser (180 s, 1400 mW/cm^2) or with a NS laser (180 s, 1400 mW/cm^2) with simultaneous temperature measurements using a thermal camera (**Figure S16**). Laser-induced hyperthermia was quantified using a setup identical to the previous one (**Figure S11**). The tumors were aligned such that the ytterbium fiber laser IRE-POLUS ILMI-1-50 (1064 nm, 100 kHz, <140 ns) and ytterbium fiber laser Antaus Avesta (1030 nm, 200 kHz, <250 fs) beams were aimed perpendicularly at the tumor. An infrared thermal imaging

camera FLIR Titanium 520 M, positioned at an angle to the laser beam's path, monitored the temperature variations within the tumor (Figure S17). Two days later, the mice were sacrificed, and the tumors were extracted.

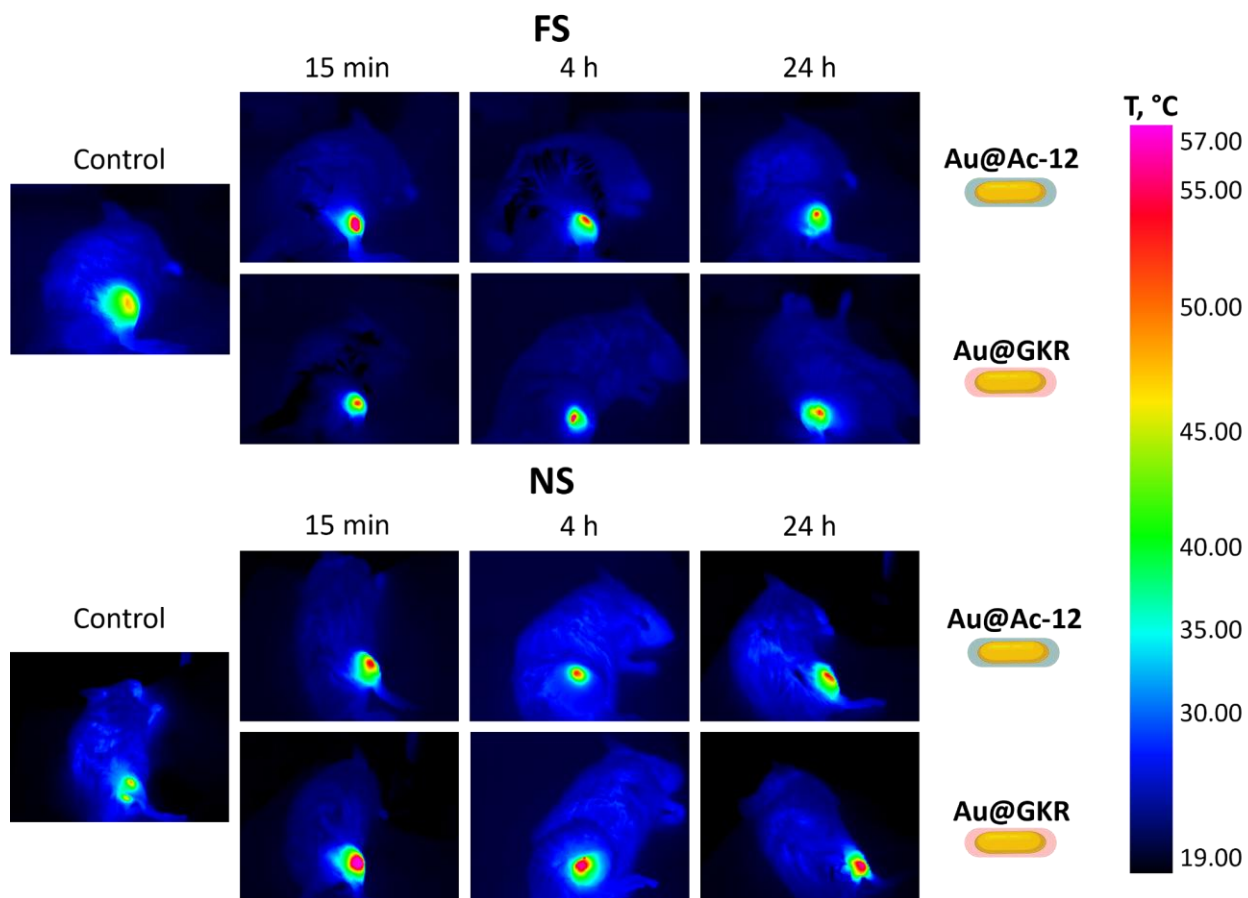


Figure S16. Thermal images of mice with intratumorally injected either **Au@Ac-12** or **Au@GKR** ($c = 1000 \mu\text{g/mL}$) irradiated with either FS or NS.

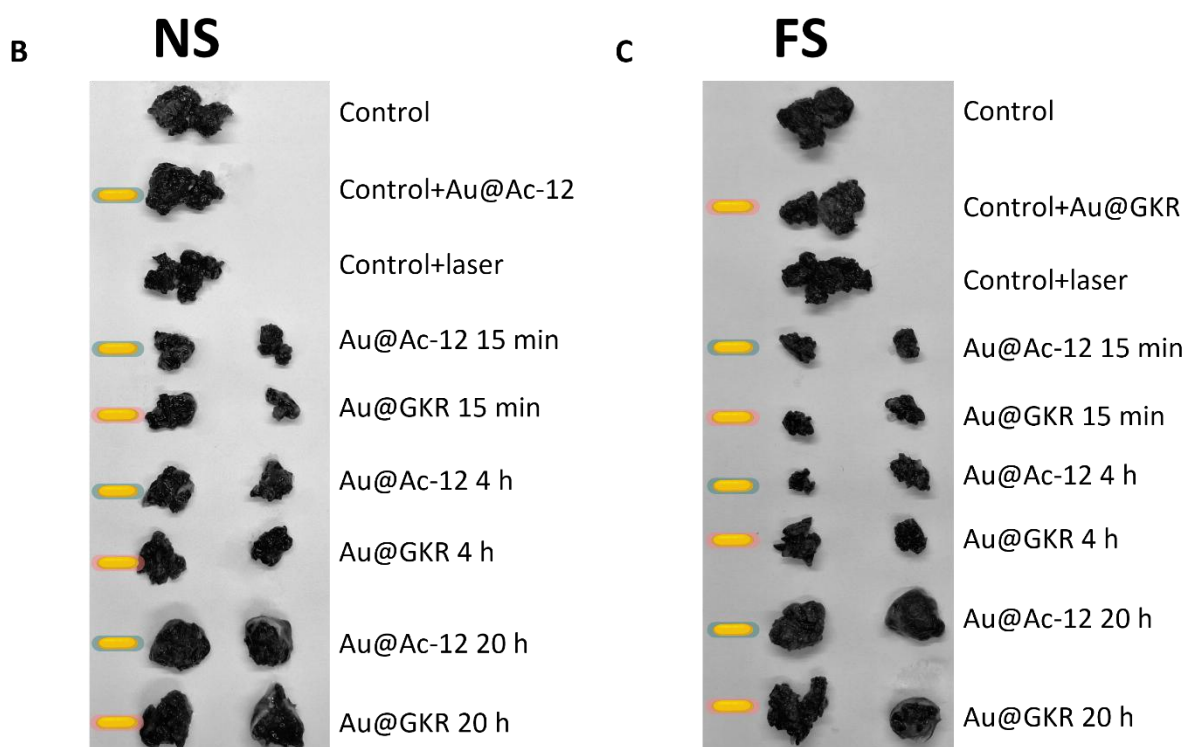
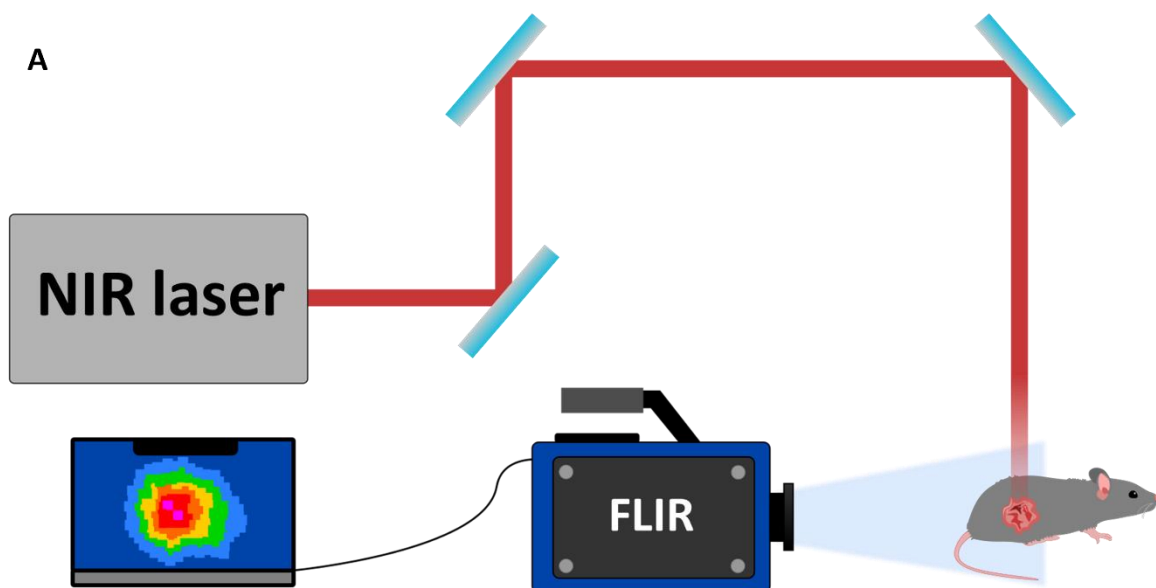


Figure S17. (A) Schematic illustration of the experimental setup for the laser-induced heating of **Au@Ac-12** and **Au@GKR** injected in melanoma-bearing mice. (B,C) Representative digital images of tumors from different mice groups (irradiated with left: NS and right: FS).

5 f. Histological analysis

For histological studies, mice were sacrificed 2 days after the therapy by cervical dislocation, and tumors were extracted and fixed in 10% normal formalin solution.

For histological examination, tumor tissues were fixated with 10% normal formalin solution. After fixation, the tissue samples were dehydrated and soaked with paraffin using isopropanol and Shandon Varistain Gemini (Thermo Shandon Ltd., UK) slide stainer. After pouring the samples

into paraffin from paraffin blocks using a rotary microtome HM-340E (Microm GmbH, Germany), 4- μ m-thick sections were cut, placed on slides, stained with hematoxylin and eosin, and immobilized under cover glasses. Histological samples were studied under transmitted light using an Axio Imager microscope (Zeiss, Germany) and scanned using a Panoramic Midi (3D) micro-preparation scanner (Histec, Hungary). The morphometric study was conducted using the Axio-Cam ICs 3 and Panoramic Viewer software (3DHISTECH Ltd., Hungary).

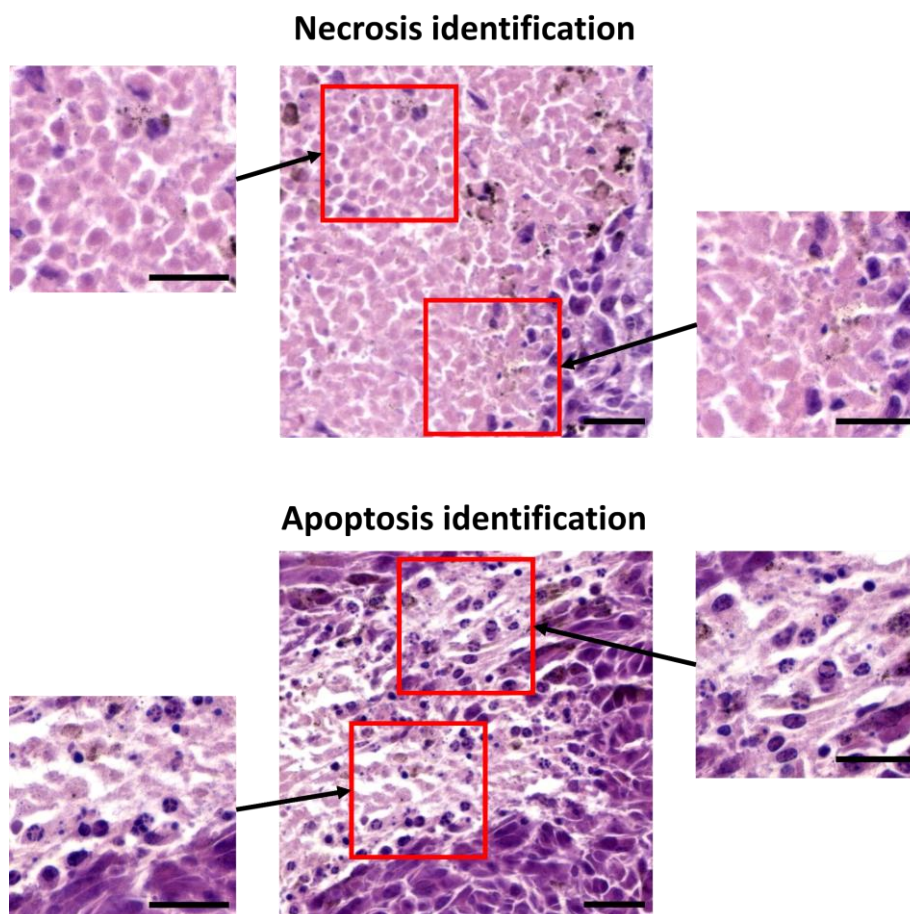


Figure S18. Representative H&E stained histological images indicating necrosis (upper part) and apoptosis (bottom part). Scale bar corresponds to 25 μ m.

6. Clinical studies review

Table S4. Registered clinical trials utilizing Au NPs for PTT.

| | Name | Identification No | Material | Condition | Enrollment | Application | Study start | Study completion | Result | Ref |
|---|---|-------------------|-------------------------------------|----------------------|------------|--|-------------|------------------|---|-----|
| 1 | Pilot Study of Auro-Lase(tm) Therapy in Refractory and/or Recurrent Tumors of the Head and Neck | NCT00848042 | PEGylated silica-gold nanoparticles | Head and neck cancer | 11 | The use of photothermal ablation of the gold nanoshells to | 2008-04 | 2014-08 | Completed: 5 Not completed: 6 (deaths : 3, other | 9 |

| | | | | | | | | | | |
|---|--|--------------------------------------|-------------------------------------|-----------------------------------|----|---|---------|---------|--|----|
| | | | | | | induce cell death in tumors while minimizing damage to surrounding healthy tissue | | | therapy: 3) | |
| 2 | Efficacy Study of Au-roLase Therapy in Subjects With Primary and/or Metastatic Lung Tumors | NCT01679470 | PEGylated silica-gold nanoparticles | Primary or Metastatic Lung Tumors | 1 | | 2012-10 | 2014-06 | No results posted | 10 |
| 3 | Initial Evaluation of the Safety of Nanoshell-Directed Photothermal Therapy in the Treatment of Prostate Disease | CAS/OR/01/CMN/103300410C00101968/201 | PEGylated silica-gold nanoparticles | Prostate cancer | 22 | Evaluation of safety profile of gold nanoshells for use in patients with prostate cancer. Specifically, to assess the clinical safety of nanoshell-directed photothermal therapy in prostate cancer patients. | - | 2016 | The study successfully demonstrated the feasibility of administering gold nanoshells intravenously and performing subsequent laser ablation in prostate cancer patients. | 11 |
| 4 | Gold nanoshell-localized photothermal ablation of prostate tumors in a clinical pilot device study | - | PEGylated silica-gold nanoparticles | Localized prostate cancer | 16 | Highly localized regional control of prostate cancer that also results in greatly reduced patient morbidity and improved functional outcomes | - | 2019 | Completed: 15 | 12 |

| | | | | | | | | | | |
|---|---|-------------|-------------------------------------|---------------------------|----|--|---------|---------|-------------------|-------|
| 5 | MRI/US Fusion Imaging and Biopsy in Combination With Nanoparticle Directed Focal Therapy for Ablation of Prostate Tissue | NCT02680535 | PEGylated silica-gold nanoparticles | Neoplasms of the Prostate | 45 | Laser-induced photothermal ablation as a focal treatment for localized prostate cancer with simultaneous MRI/ultrasound fusion imaging | 2016-02 | 2020-10 | No results posted | 13,14 |
| 6 | An Extension Study MRI/US Fusion Imaging and Biopsy in Combination With Nanoparticle Directed Focal Therapy for Ablation of Prostate Tissue | NCT04240639 | PEGylated silica-gold nanoparticles | Neoplasms of the Prostate | 60 | MRI/ultrasound fusion imaging combined with nanoparticle-targeted focal therapy for the ablation of prostate tissue | 2020-01 | 2023-06 | No results posted | 15,16 |

REFERENCES

- (1) Ye, X.; Zheng, C.; Chen, J.; Gao, Y.; Murray, C. B. Using Binary Surfactant Mixtures To Simultaneously Improve the Dimensional Tunability and Monodispersity in the Seeded Growth of Gold Nanorods. *Nano Lett.* **2013**, *13* (2), 765–771. <https://doi.org/10.1021/nl304478h>.
- (2) Park, K.; Hsiao, M.-S.; Koerner, H.; Jawaid, A.; Che, J.; Vaia, R. A. Optimizing Seed Aging for Single Crystal Gold Nanorod Growth: The Critical Role of Gold Nanocluster Crystal Structure. *J. Phys. Chem. C* **2016**, *120* (49), 28235–28245. <https://doi.org/10.1021/acs.jpcc.6b08509>.
- (3) Nafisah, S.; Morsin, M.; Jumadi, N. A.; Nayan, N.; Shah, N. Z. A. M.; Razali, N. L.; Soon, C. F. Seed-Mediated Growth of Gold Nanorods Using Silver Seeds: Effect of Silver Seeds Concentration and Growth Time. *Int. J. Eng. Technol.* **2018**, *7* (4.30), 121. <https://doi.org/10.14419/ijet.v7i4.30.22071>.
- (4) Gong, X. W.; Wei, D. Z.; He, M. L.; Xiong, Y. C. Discarded Free PEG-Based Assay for Obtaining the Modification Extent of Pegylated Proteins. *Talanta* **2007**, *71* (1), 381–384. <https://doi.org/10.1016/j.talanta.2006.04.010>.
- (5) Bartczak, D.; Kanaras, A. G. Preparation of Peptide-Functionalized Gold Nanoparticles Using One Pot EDC/Sulfo-NHS Coupling. *Langmuir* **2011**, *27* (16), 10119–10123. <https://doi.org/10.1021/la2022177>.
- (6) Tenland, E.; Pochert, A.; Krishnan, N.; Rao, K. U.; Kalsum, S.; Braun, K.; Glegola-Madejska, I.; Lerm, M.; Robertson, B. D.; Lindén, M.; Godaly, G. Effective Delivery of the Anti-Mycobacterial Peptide NZX in Mesoporous Silica Nanoparticles. *PLOS ONE* **2019**, *14* (2), e0212858. <https://doi.org/10.1371/journal.pone.0212858>.
- (7) Orendorff, C. J.; Murphy, C. J. Quantitation of Metal Content in the Silver-Assisted Growth of Gold Nanorods. *J. Phys. Chem. B* **2006**, *110* (9), 3990–3994. <https://doi.org/10.1021/jp0570972>.
- (8) Liu, X.; Li, B.; Fu, F.; Xu, K.; Zou, R.; Wang, Q.; Zhang, B.; Chen, Z.; Hu, J. Facile Synthesis of Biocompatible Cysteine-Coated CuS Nanoparticles with High Photothermal Conversion Efficiency for Cancer Therapy. *Dalton Trans.* **2014**, *43* (30), 11709–11715. <https://doi.org/10.1039/C4DT00424H>.
- (9) *Study Details | Pilot Study of AuroLase(tm) Therapy in Refractory and/or Recurrent Tumors of the Head and Neck | ClinicalTrials.gov.* <https://clinicaltrials.gov/study/NCT00848042> (accessed 2024-09-10).
- (10) *Study Details | Efficacy Study of AuroLase Therapy in Subjects With Primary and/or Metastatic Lung Tumors | ClinicalTrials.gov.* <https://clinicaltrials.gov/study/NCT01679470> (accessed 2024-09-10).
- (11) Stern, J. M.; Solomonov, V. V. K.; Sazykina, E.; Schwartz, J. A.; Gad, S. C.; Goodrich, G. P. Initial Evaluation of the Safety of Nanoshell-Directed Photothermal Therapy in the Treatment of Prostate Disease. *Int. J. Toxicol.* **2015**. <https://doi.org/10.1177/1091581815600170>.
- (12) Rastinehad, A. R.; Anastos, H.; Wajswol, E.; Winoker, J. S.; Sfakianos, J. P.; Doppalapudi, S. K.; Carrick, M. R.; Knauer, C. J.; Taouli, B.; Lewis, S. C.; Tewari, A. K.; Schwartz, J. A.; Canfield, S. E.; George, A. K.; West, J. L.; Halas, N. J. Gold Nanoshell-Localized Photothermal Ablation of Prostate Tumors in a Clinical Pilot Device Study. *Proc. Natl. Acad. Sci.* **2019**, *116* (37), 18590–18596. <https://doi.org/10.1073/pnas.1906929116>.
- (13) *Study Details | MRI/US Fusion Imaging and Biopsy in Combination With Nanoparticle Directed Focal Therapy for Ablation of Prostate Tissue | ClinicalTrials.gov.* <https://clinicaltrials.gov/study/NCT02680535> (accessed 2024-09-10).
- (14) Jue, J. S.; Coons, S.; Hautvast, G.; Thompson, S. F.; Geraats, J.; Richstone, L.; Schwartz, M. J.; Rastinehad, A. R. Novel Automated Three-Dimensional Surgical Planning Tool and Magnetic Resonance Imaging/Ultrasound Fusion Technology to Perform Nanoparticle Ablation and Cryoablation of the Prostate for Focal Therapy. *J. Endourol.* **2022**. <https://doi.org/10.1089/end.2021.0266>.
- (15) *Study Details | An Extension Study MRI/US Fusion Imaging and Biopsy in Combination With Nanoparticle Directed Focal Therapy for Ablation of Prostate Tissue | ClinicalTrials.gov.* <https://clinicaltrials.gov/study/NCT04240639> (accessed 2024-09-10).

- (16) Kadria-Vili, Y.; Schwartz, J. A.; Polascik, T. J.; Goodrich, G. P.; Jordan, D.; Pinder, D.; Halas, N. J.; Rastinehad, A. R. A Detailed Clinical Case of Localized Prostate Tumors Treated with Nanoparticle-Assisted Sub-Ablative Laser Ablation. *Nanomaterials* **2024**, *14* (15), 1261. <https://doi.org/10.3390/nano14151261>.